Clays and Clay Minerals, Vol. 66, No. 3, 233–244, 2018.

ISOTHERMAL CRYSTALLIZATION PROPERTIES AND IMPROVED RHEOLOGICAL PERFORMANCE OF WAXY CRUDE OIL USING POLYOCTADECYLACRYLATE-MODIFIED MONTMORILLONITE COMPOSITE AS A POUR POINT DEPRESSANT

Bo Yao[1,2], Chuanxian Li[1,2], Fei Yang[1,2,*], and Guangyu Sun[1,2]

[1] College of Pipeline and Civil Engineering, China University of Petroleum, Qingdao, Shandong 266580, P.R.C.
[2] Shandong Provincial Key Laboratory of Oil & Gas Storage and Transportation Safety, Qingdao, Shandong 266580, P.R.C.

Abstract—Recently, studies on the use of polymer nanomaterial composites as pour-point depressants (PPD) have drawn much attention, but the crystallization properties and improved rheological performance of waxy crude oils using nanoclay-based composite PPDs have rarely been reported. In this paper, montmorillonite (Mnt) was first organically modified using octadecyltrimethylammonium chloride ($C_{21}H_{46}NCl$, or stearyltrimethylammonium chloride) in aqueous solution. Then, the organically modified Mnt (OMnt) material was dispersed into a polyoctadecylacrylate (POA) matrix to prepare a POA/OMnt composite PPD by melt blending. The composition, structure, and morphology of Mnt, OMnt, and the POA/OMnt composite PPDs were investigated. The results showed that the OMnt and POA were compatible and that the OMnt was exfoliated into several sheets in the POA matrix. Subsequently, the isothermal crystallization kinetics of the POA/OMnt composite PPDs showed that small amounts of OMnt had a dramatic impact on POA chain motion during crystallization and facilitated POA crystallization. After it was added to a waxy crude oil, the POA/OMnt composite PPDs produced better rheological properties and performance than identical concentrations of the neat POA. The POA/OMnt composite PPDs can act as wax nucleation sites for wax molecule precipitation and result in larger and more compact wax crystal flocs, which adversely affect the formation of a wax crystal network and, thus, favor the improvement of waxy crude oil rheology.

Key Words—Isothermal Crystallization Kinetics, Nanocomposite Pour Point Depressant, Organically Modified Montmorillonite, Waxy Crude Oil.

INTRODUCTION

A typical waxy crude oil contains large amounts of paraffin waxes, which trigger huge challenges in oil recovery, processing, storage, and transportation (Lashkarbolooki *et al.*, 2010). The paraffin waxes can precipitate below the crude oil wax appearance temperature (WAT) to form wax crystals, which can complicate the oil rheological properties. With a further decrease in temperature to the crude oil pour point, the amounts of precipitated wax crystals can accumulate to a certain extent and interlock together to form a continuous wax crystal network. When the crude oil temperature decreases to the pour point, the flow in pipelines can be stopped due to the decreased oil mobility. One of the recognized and efficient ways to alleviate these problems is to add polymeric pour point depressants (PPDs) into the waxy crude oil (Yang *et al.*, 2015b; Yao *et al.*, 2018a). PPDs are chemical additives that are used to modify the viscosity and yield stress of crude oil by changing the shape of the wax crystals that form as the oil is cooled. Polymeric PPDs added to waxy crude oils can modify wax crystal growth habits by nucleation, adsorption, and co-crystallization effects and effectively inhibit the tendency of wax crystals to interlock into three-dimensional networks. Consequently, the pour point, viscosity, and yield stress values of waxy crude oils with added PPDs are substantially reduced (Xu *et al.*, 2015; Oliveira *et al.*, 2016). Polyoctadecylacrylate (POA, $C_{22}H_{42}O_2$) is an effective comb-like PPD for waxy crudes that appears to favor the formation of island defects on paraffin wax surfaces. POA weakly interacts with surrounding wax crystals and, therefore, acts as an impurity site to block growth steps. The morphologies of the POA contaminated wax crystals, therefore, are greatly modified and the rheological properties of the crude oil are significantly improved (Yao *et al.*, 2017).

On the one hand, research on PPDs has focused on the crystallization properties of PPDs or waxes and has aimed to identify the interaction mechanism of PPDs and other components in the waxy crude oil (Yi and Zhang, 2011). On the other hand, research has explored or developed novel PPDs with a better performance for use in waxy crude oil recovery. Recently, application of nanomaterials in traditional polymeric PPDs to prepare more efficient nanocomposite PPDs has become a "hot" topic. Yang *et al.* (2015a) prepared a nanohybrid PPD by directly dispersing hydrophilic nanosilica into POA PPDs. Compared to POA-based PPDs, the nanohybrid PPD further reduced the gelation point, viscosity, and yield stress of synthetic waxy oils, but the hydrophobic POA molecules and hydrophilic nanosilica are not

* E-mail address of corresponding author:
yangfei@upc.edu.cn
DOI: 10.1346/CCMN.2018.064095

compatible and suppress the time effectiveness of the hybrid PPD. To make the nanomaterials and the organic phase compatible, a series of polymethylsilsesquioxane (PMSQ) microspheres were synthesized and the PMSQ microspheres were dispersed into poly(ethylene-vinyl acetate) (EVA) PPDs (Yang *et al.*, 2017a, 2017b; Yao *et al.*, 2017, 2018b). The EVA molecules can be adsorbed to and concentrate on PMSQ microspheres and, thus, cause the formation of EVA/PMSQ composite particles. The composite particles can act as nucleation templates for wax precipitation to form larger and more compact wax microstructures, which can further improve the oil flow behavior.

Montmorillonite (Mnt) is a layered silicate mineral with a 2:1 type layer structure (Wang *et al.*, 2003; Khajehpour *et al.*, 2015; Chen *et al.*, 2017). Due to isomorphous cation substitutions, Mnt is negatively charged and hydrated Na^+ or Ca^{2+} interlayer cations balance the negative charge (*i.e.* Na^+-Mnt or Ca^{2+}-Mnt). Surfactants, such as quaternary ammonium salts, can replace the interlayer hydrated Na^+ or Ca^{2+} through cation exchange, enlarge layer spacing, and enhance the lipophilicity of Mnt. In this way, the organically modified Mnt (OMnt) is easier to disperse in a polymer matrix and is more compatible with the organic phase (He *et al.*, 2005). Al-Sabagh *et al.* (2016) successfully prepared poly(methylmethacrylate)/montmorillonite (PMMA/Mnt) nanocomposite PPDs by dispersing the inorganic nanolayers of Mnt in the organic PMMA matrix *via in situ* free radical polymerization. Al-Sabagh *et al.* (2016) found that the nanocomposite PPD dispersed well in the oil phase as small composite particles and that the performance of the nanocomposite PPD was much better than the neat PMMA PPD. Al-Sabagh *et al.* (2016) attributed the excellent performance of the nanocomposite PPD to the nucleation effect of the composite particles and electrostatic repulsion between the composite particles. Yao *et al*. (2016a) first prepared organically modified nanoclays (abbreviated as organic nanoclays) through cationic exchange and then dispersed the organic nanoclays into a POA PPD matrix. The POA/organic clay nanocomposite PPD that was formed dispersed well in an oil phase as small composite particles (several microns) and the composite particles also acted as nucleation templates for wax precipitation. The morphology of the precipitated wax crystals, therefore, was greatly modified after the addition of the nanocomposite PPD and resulted in further improvement in the rheology of waxy crude oil. In addition, the time-effectiveness of the POA/organic clay nanocomposite PPD was also greatly improved.

The effects of OMnt on the isothermal crystallization properties of POA/OMnt composite PPDs have not been reported, however, and the mechanism of action and the improved rheological performance of POA/OMnt composite PPDs for waxy crude oil should be further studied. The aim of the present work, therefore, was to answer the questions mentioned above.

MATERIALS AND METHODS

Materials

The OTAC, 2,2′-Azobis(2-methylpropionitrile) (AIBN), toluene, ethanol, and octadecyl acrylate (OA) were purchased from Sinopharm Chemical Reagent Co., Shanghai, China. Deionized water was purified by reverse osmosis. The comb-like POA PPDs were synthesized by the solvent free-radical polymerization of OA using the method of Yao *et al.*, (2016b). The average molecular weight of POA measured by gel permeation chromatography (GPC) was around 20,000 Da. The synthesized POA polymer was analyzed by ^{1}H nuclear magnetic resonance (NMR) using a Bruker Avance 500 NMR spectrometer (Bruker Corporation, Billerica, Massachusetts, USA) with deuterated chloroform as solvent (Figure 1). Chemical shifts of 4.0, 1.62, 1.3, and 0.9 ppm were found for (a) $-C=O-CH_2-$, (b) $-CH-$, (c) $-CH_2-$, and (d) $-CH_3$ protons, respectively. The untreated Mnt sample was purchased from Hengshi Mineral Processing Co., Shijiazhuang, China. The cation exchange capacity (CEC) of the Mnt nanoclay was around 98 mmol/100 g. The OMnt was intercalated with OTAC *via* cation exchange in an aqueous solution using the method of Yao *et al.* (2016a). The OTAC concentration was fixed at 1.5 times the nanoclay CEC. The composition and structure of the organic nanoclay were analyzed using a Nicolet iS5 FTIR spectrometer (Thermo Fisher Scientific, Waltham, Massachusetts, USA) and X'Pert Pro X-ray diffractometer (PANalytical, Almelo, The Netherlands), respectively.

The crude oil was kindly provided and obtained from the Changqing oil field in China. According to the composition analysis of the crude oil, the Changqing crude oil contains 15.79% wax, 0.57% asphaltene, and 7.48 wt.% resin, which means that the Changqing crude oil is a typical waxy crude oil.

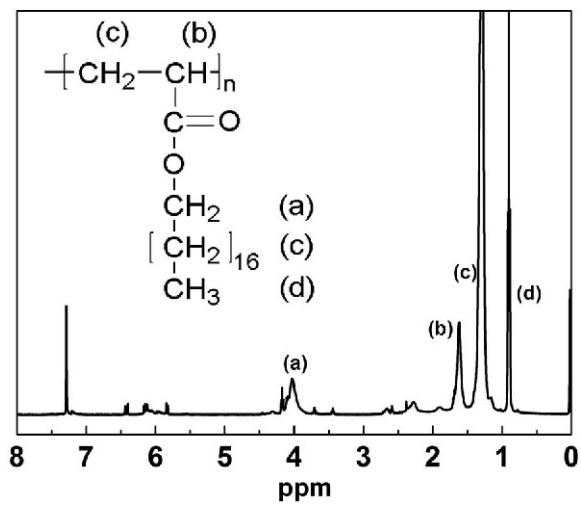

Figure 1. ^{1}H NMR spectrum of synthesized POA polymer.

https://doi.org/10.1346/CCMN.2018.064095 Published online by Cambridge University Press

Preparation and characterization of POA/OMnt composite PPD

The POA/OMnt composite PPD was prepared using a melt blending method. The mass ratios of OMnt in the composite PPDs were 0.5%, 2%, 5%, and 10 wt.%. The composition and structure of the composite PPDs were analyzed using FTIR and XRD. CuKα X-ray radiation was used with a scanning rate of 1º2θ/min and a scanning range of 3º2θ to 15º2θ. The composite PPD morphologies were observed using a Hitachi S-480 scanning electron microscope (SEM) (Hitachi Co., Tokyo, Japan). The dispersion state of the composite PPDs in *n*-dodecane were assessed using a JEOL JEM-100CX transmission electron microscope (TEM) (JEOL Co., Tokyo, Japan).

Isothermal crystallization kinetics of the POA/OMnt composite PPDs

The crystallization behaviors of the POA/OMnt composite PPDs were investigated by using a Mettler DSC 821e differential scanning calorimeter (Mettler Toledo Co., Columbus, Ohio, USA) under a N_2 atmosphere. Each sample was encapsulated in a closed Al pan with a fixed weight of 6−9 mg. To eliminate the thermo-mechanical history, the samples were melted at 140ºC and held at that temperature for 5 min. Then, the samples were cooled rapidly from 140ºC to the isothermal crystallization temperature T_c of 37 to 45ºC and maintained at the T_c until the maximum degree of crystallization was completed (Liu *et al.*, 2014; Shi and Dou., 2015; Shivdel Ghadikolaei *et al.*, 2016). Accordingly, the crystallization enthalpies H as a function of time t were obtained to determine the crystallization characteristics.

From the DSC curves, the relative crystallinity α as a function of time can be calculated according to equation 1:

$$\alpha = \frac{\int_{t_{onset}}^{t} \frac{dH}{dt} dt}{\int_{t_{onset}}^{t_{endset}} \frac{dH}{dt} dt} \quad (1)$$

where t, t_{onset}, and t_{endset} denote the instantaneous, onset, and endset crystallization times, respectively, and dH denotes the change of enthalpy over a dt time interval.

Flow behavior tests of the untreated/PPD-treated waxy crude oil

Pour point test. The pour points of the waxy crude oil samples that were either untreated or treated with the POA and POA/OMnt composite PPDs were measured using the Chinese Standard SY/T 0541-2009 method (Yao *et al*., 2017) and the preheat treatment temperature was fixed at 60ºC.

Transient flow curve test. The untreated and PPD-treated waxy crude oils were cooled quiescently under the cooling rate of 0.5ºC/min from 60ºC to 10ºC and then maintained isothermally at 10ºC for 30 min. Subsequently, transient flow curves of the oil samples were measured at 10ºC by ramping the shear rate from 1 to 300 s^{-1} within 10 min. Variations in the transient apparent viscosity with shear rate were recorded.

Yield behavior test. The untreated and PPD-treated waxy crude oils were also cooled quiescently from 60ºC to 10ºC with a fixed cooling rate of 0.5ºC/min and then maintained isothermally at 10ºC for 30 min. After that, the yield behaviors of the oil samples were measured at 10ºC by linearly ramping the shear stress from 0 to 200 Pa within 40 min. The variations in the strain with shear stress were recorded. The yield stress values were determined at the shear stress value when a dramatic increase of the shear strain occurred.

Polarized microscope observation test. An Olympus BX51 polarized microscope (Olympus Co., Tokyo, Japan) fitted with an automatic thermal stage was used to observe wax crystals that precipitated from the crude oil. After being pre-heated to 60ºC for the same time, one droplet of the crude oil sample was transferred to a glass slide and covered with a coverslip. The crude oil sample glass slides were cooled from 60ºC to 10ºC on the microscope stage using a fixed cooling rate of 0.5ºC/min and the morphology of the precipitated wax crystals was photographed at 10ºC.

RESULTS AND DISCUSSION

Structure and morphology of the OMnt and POA/OMnt composite PPDs

The X-ray powder diffraction patterns of the untreated Mnt sample and the organically modified Mnt (OMnt) samples (Figure 2) were used with the Bragg equation, $n\lambda = 2d\sin\theta$, to calculate the basal spacings of Mnt. The d_{001} value of untreated Mnt was 1.513 nm, but the d_{001} value

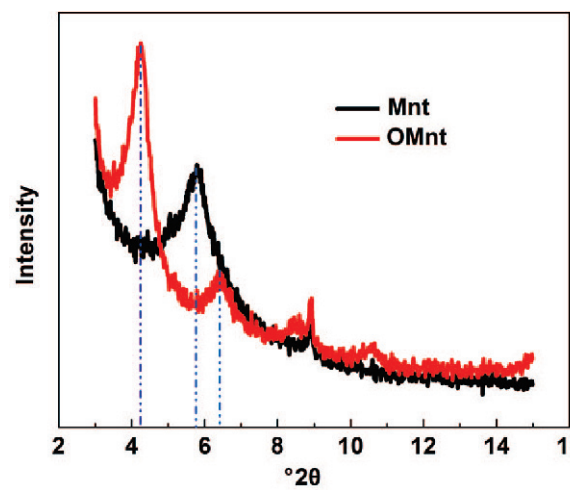

Figure 2. XRD patterns of Mnt and OMnt.

https://doi.org/10.1346/CCMN.2018.064095 Published online by Cambridge University Press

of OMnt was 1.964 nm and d_{002} peaks were apparent. This confirmed that the cationic surfactant OTAC molecules with eighteen side alkyl chains were successfully intercalated into Mnt interlayers.

The FTIR spectra of the untreated Mnt, OMnt, and POA/OMnt composite PPD (2 wt.%) samples (Figure 3a) revealed that the untreated Mnt nanoclay displayed characteristic absorption bands at 1100 cm^{-1} (Si-O-Si antisymmetric stretching vibration), 474 cm^{-1} (SiO_2 stretching), and 3400~3230 cm^{-1} (R-O-H stretching). In the FTIR spectrum of the organic nanoclay, the C-N absorption band at 1250 cm^{-1} confirmed that OTAC adsorbed to the outer surfaces and interlayers of the nanoclay *via* ion exchange. The POA/OMnt composite

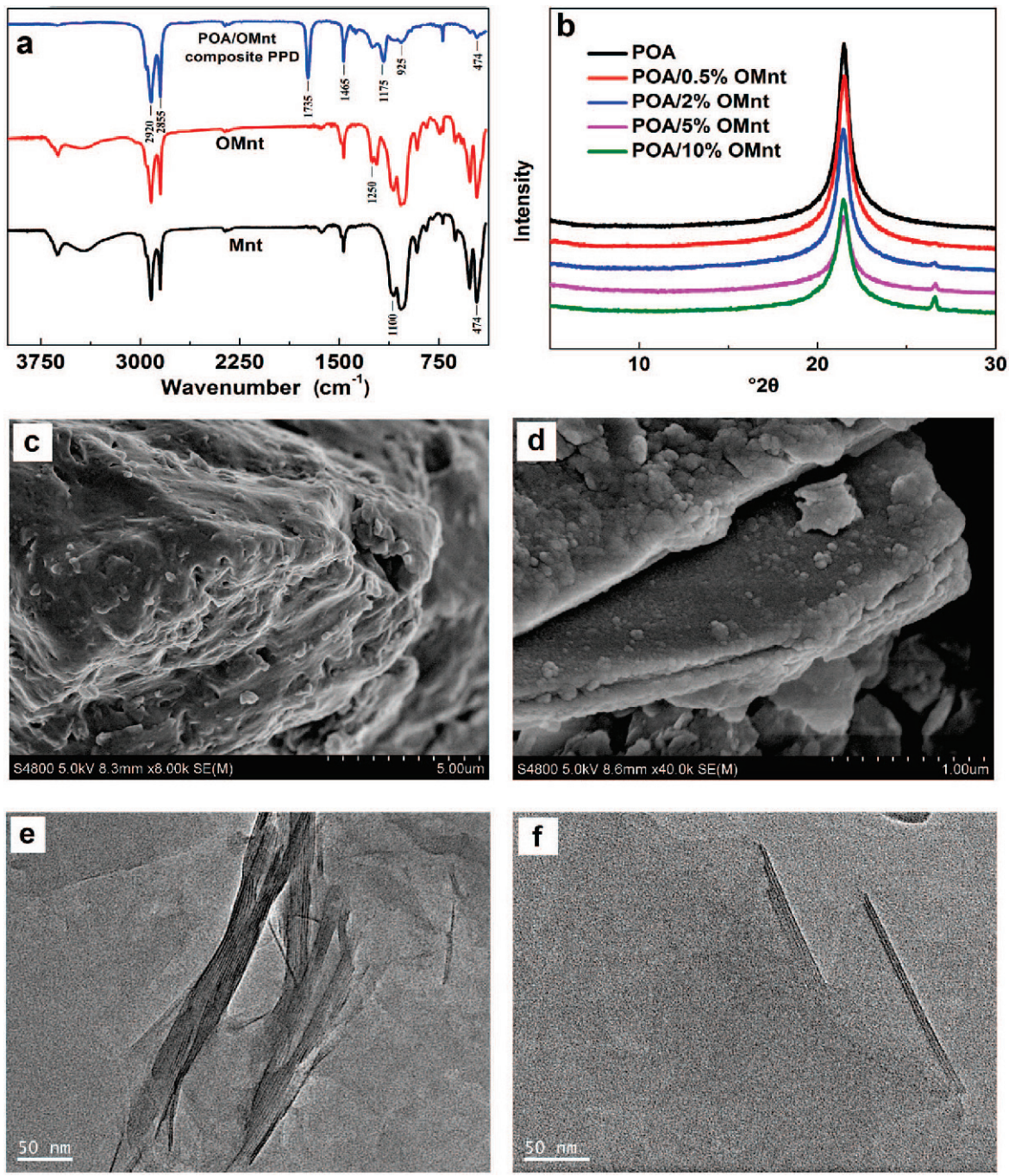

Figure 3. (a) FTIR spectra of Mnt, OMnt, and POA/OMnt composite PPD ; (b) XRD patterns of POA and POA/OMnt; (c, d) SEM micrographs of POA/OMnt composite PPD; (e) TEM images of Mnt; and (f) POA/OMnt composite PPD with 5 wt.% OMnt.

https://doi.org/10.1346/CCMN.2018.064095 Published online by Cambridge University Press

PPD displayed characteristic absorption bands at 2920cm^{-1} (-CH_3 characteristic peak), 925 cm^{-1}, 1465 cm^{-1}, 2855 cm^{-1} (-CH_2- characteristic peak), 1735 cm^{-1} (C=O stretching in ester), and 1175 cm^{-1} (C-O-C stretching). The peaks at 1100 cm^{-1} (Si-O-Si stretching), 802 cm^{-1}, and 474 cm^{-1} (SiO_2 characteristic peak) observed for Mnt were retained. Wide-angle X-ray diffraction spectra of POA and POA/OMnt composite PPDs in the 0−30º2θ range (Figure 3b) showed only one or two distinct peaks and no diffuse peaks, which verified the crystal structures of the POA and POA/OMnt composite PPDs. The peak at 26.50º2θ was due to α-quartz and the peak height increased with increased OMnt contents. Basal peaks for OMnt (⩽10º2θ) were not observed, but a regular and sharp peak at 21.48º2θ (due to the C_{18} side chain of POA) was observed in all sample spectra. This indicates that the chemical bonding and aggregation of POA was not affected by the OMnt and OMnt layer structures because the clays were exfoliated into several sheets. Furthermore, the SEM images of the POA/OMnt composite PPD in Figure 3c and 3d indicated that POA was more compatible with OMnt. Some POA grew with the OMnt sheet and intercalated into the OMnt layers and some OMnt sheets dispersed into the POA matrix. The untreated Mnt is a natural inorganic material and the untreated Mnt has poor compatibility with the organic phase, which has been noted in many published works (Yao *et al*., 2016a, 2016b). After the organic modification, the surfaces and interlayers of Mnt had many grafted alkane chains due to the cation exchange reaction and the interactions between the Mnt layers were significantly weakened. The OMnt can, therefore, interact with the organic phase by van der Waals forces and then disperse well in the polymer matrix. In other words, the OMnt and POA components are very compatible (Li *et al*., 2006; Page and Adachi, 2006). All the above data confirm the successful preparation of a POA/OMnt composite PPD. The exfoliated OMnt sheets can be more clearly seen in the TEM images of the POA/OMnt composite PPD (Figures 3e and 3f).

Isothermal crystallization kinetics of POA/OMnt composite PPDs

The isothermal crystallization curves of POA/OMnt composite PPDs that contain different OMnt contents at different isothermal temperatures (Figure 4) had curves that shifted to lower time values and became sharper and narrower with a decreased isothermal crystallization temperature. This means that increased supercooling was the driving force of crystallization and accelerated the crystallization process.

The Avrami equation (Avrami, 1940; Sadek *et al*., 2015) has been widely applied to describe the kinetics of isothermal crystallization and is shown in equations 2 and 3:

$$1 - \alpha = \exp(-Z_t t^n) \quad (2)$$

$$\ln(-\ln(1 - \alpha)) = \ln Z_t + n \ln t \quad (3)$$

where Z_t is the crystallization rate constant that involves crystal growth and the nucleation rate and n is the Avrami constant that depicts the crystal growth mechanism and dimensional geometry. Equation 1 can be used to calculate the α values and used to plot $\ln(-\ln(1 - \alpha))$ *vs.* $\ln t$ curves for the POA/OMnt composite PPDs that contain different OMnt contents at different isothermal temperatures (Figure 5). During the time for initial crystallization ($\alpha \leqslant 70\%$), the crystal sizes were relatively small and the crystals grew separately. Thus, the $\ln(-\ln(1 - \alpha))$ values had a good linear relationship with $\ln t$. By fitting the $\ln(-\ln(1 - \alpha))$ *vs.* $\ln t$ plots to a line, the Z_t and n values for different composites at different isothermal temperatures were obtained and are listed in Table 1. As the crystallization process proceeds, however, $\ln(-\ln(1 - \alpha))$ no longer had a strict linear relationship with $\ln t$. This means that the crystallization rate was affected by the increased size of the crystals and that the crystallization process at this stage could not be precisely described using the Avrami equation. The Avrami constant, n, is directly related to crystal nucleation, crystal growth, and equal to the sum of the time and space dimensions of the two processes (see Table 2). As shown in Table 2, heterogeneous nucleation is the adsorption of an ordered polymer chain with some impurities, such as pre-crystals or small solid particles. Heterogeneous nucleation is generally instantaneous, is time independent, and has a time dimension of 0. When no heterogeneous nucleation sites are available, the homogeneous nucleation process is triggered by the thermal motions of the polymer chains, is largely time dependent, and the time dimension is 1. The space dimensions are 1, 2, and 3, which represent one-, two-, and three-dimensional growth, respectively. According to theory, the Avrami constant n should be an integer. The crystallization temperature, the thermal history, and a variety of nucleation and growth processes, however, resulted in non-integral properties. For POA/OMnt composite PPDs with different OMnt contents, therefore, the nucleation processes were heterogeneous nucleation and the growth processes were the one-dimensional growth of acicular crystals into two-dimensional crystals.

The crystallization half time $t_{1/2}$ and maximum crystallization rate time t_{max} can be calculated using equations 4 and 5, respectively, and are listed in Table 1. The $t_{1/2}$ isothermal temperature curves and t_{max} isothermal temperature curves are illustrated in Figure 6.

$$t_{1/2} = \left(\frac{\ln 2}{Z_c}\right)^{1/n} \quad (4)$$

$$t_{max} = \left(\frac{n-1}{nZ_c}\right)^{1/n} \quad (5)$$

https://doi.org/10.1346/CCMN.2018.064095 Published online by Cambridge University Press

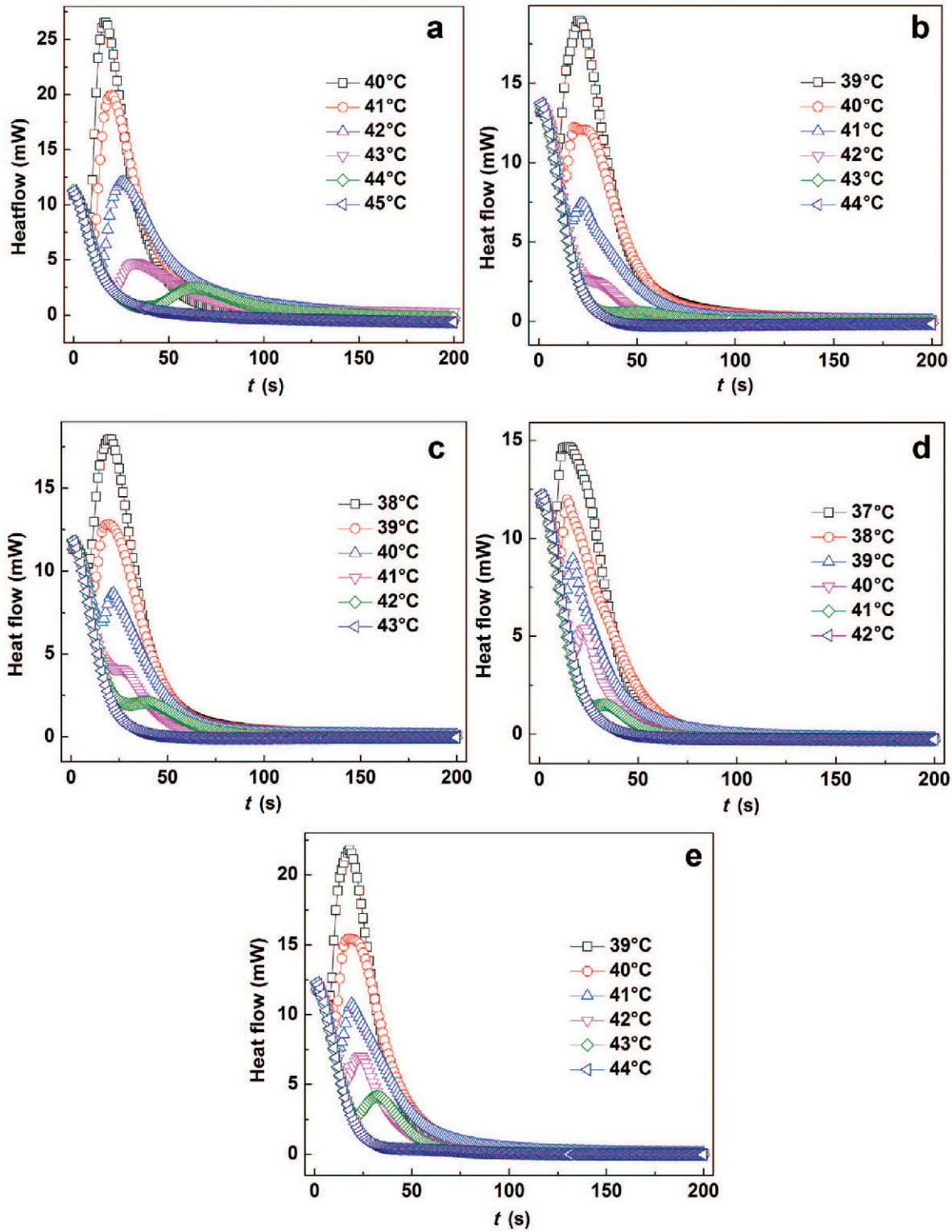

Figure 4. Isothermal crystallization curves of the POA/OMnt composite PPD at different temperatures: (a) POA; (b) POA/0.5%OMnt; (c) POA/2%OMnt; (d) POA/5%OMnt; and (e) POA/10%Mnt.

https://doi.org/10.1346/CCMN.2018.064095 Published online by Cambridge University Press

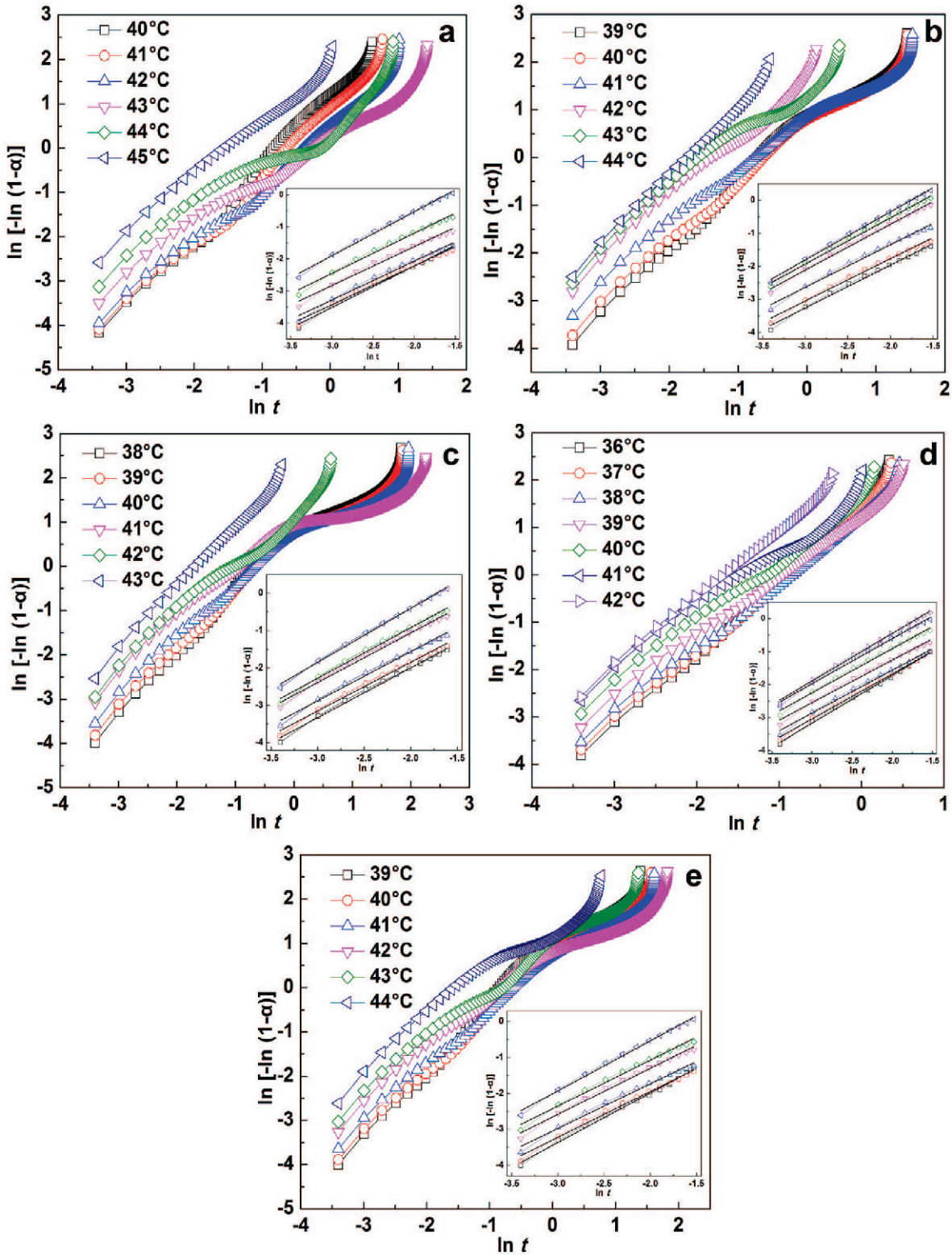

Figure 5. Plots of $\ln(-\ln(1-\alpha))$ *vs.* $\ln t$ for the POA/OMnt composite PPD at different temperatures: (a) POA; (b) POA/0.5%OMnt; (c) POA/2%OMnt; (d) POA/5%OMnt; and (e) POA/10%Mnt.

https://doi.org/10.1346/CCMN.2018.064095 Published online by Cambridge University Press

Table 1. Fit of isothermal crystallization kinetics parameters to POA/OMnt composite PPDs.

Sample	T_c (°C)	n	Z_c	$t_{1/2}$ (min)	t_{max} (min)	E (kJ·mol^{-1})
POA	40	1.29	1.44	0.57	0.24	303.3
	41	1.21	1.22	0.63	0.20	
	42	1.21	1.42	0.55	0.18	
	43	1.21	2.24	0.38	0.12	
	44	1.26	3.72	0.26	0.10	
	45	1.37	9.12	0.15	0.08	
POA/0.5%OMnt	39	1.30	1.88	0.46	0.20	6242.7
	40	1.28	2.22	0.40	0.17	
	41	1.29	3.46	0.29	0.12	
	42	1.39	7.78	0.18	0.09	
	43	1.41	9.77	0.15	0.08	
	44	1.46	13.0	0.13	0.08	
POA/2%OMnt	38	1.33	1.93	0.46	0.21	232.0
	39	1.29	2.05	0.43	0.18	
	40	1.30	2.76	0.34	0.15	
	41	1.31	4.66	0.23	0.10	
	42	1.33	5.66	0.21	0.10	
	43	1.44	11.7	0.14	0.08	
POA/5%OMnt	36	1.45	3.27	0.34	0.20	188.6
	37	1.37	2.88	0.35	0.18	
	38	1.30	2.83	0.34	0.15	
	39	1.29	3.78	0.27	0.11	
	40	1.34	5.89	0.20	0.10	
	41	1.37	8.45	0.16	0.08	
	42	1.44	11.5	0.14	0.08	
POA/10%OMnt	39	1.38	2.19	0.44	0.23	233.2
	40	1.28	1.85	0.47	0.19	
	41	1.25	2.15	0.40	0.15	
	42	1.29	3.57	0.28	0.12	
	43	1.28	4.45	0.23	0.10	
	44	1.39	9.51	0.15	0.08	

Apparently, the $t_{1/2}$ and t_{max} values of the neat POA PPD samples at the same isothermal temperature were both larger than the values for the POA/OMnt composite PPDs, which means that the addition of OMnt effectively increased the crystallization rate. Compared to POA, less time is required for the POA/OMnt composites to reach the same degree of crystallinity. For the POA/OMnt composite PPDs, the $t_{1/2}$ and t_{max} values first decreased as the OMnt (0.5−5 wt.%) content was increased and then increased with greater OMnt contents. This might be explained by noting that as the OMnt content in the POA/OMnt composite PPD increased from 0.5 to 5 wt.%, the OMnt readily dispersed into the POA matrix. This facilitated the accelerated crystallization of POA. When the OMnt content increased to 10 wt.%, however, the proportion of the inorganic material phase (solid) was quite large, had a negative impact on the melt blending process, and adversely affected the dispersion of OMnt in the POA matrix. The poor dispersion of OMnt in the POA matrix impaired the OMnt/POA crystallization process and slightly increased the $t_{1/2}$ and t_{max} values.

Assuming that the crystallization process is a thermal activation process, the apparent crystallization activation

Table 2. The Avrami constants of crystallization with different nucleation and crystal growth processes.

Growth type	Homogeneous nucleation	Heterogeneous nucleation
One-dimensional (needle-like)	$n = 1 + 1 = 2$	$n = 1 + 0 = 1$
Two-dimensional (lamellar-crystal)	$n = 2 + 1 = 3$	$n = 2 + 0 = 2$
Three-dimensional (spheroidal-crystal)	$n = 3 + 1 = 4$	$n = 3 + 0 = 3$

https://doi.org/10.1346/CCMN.2018.064095 Published online by Cambridge University Press

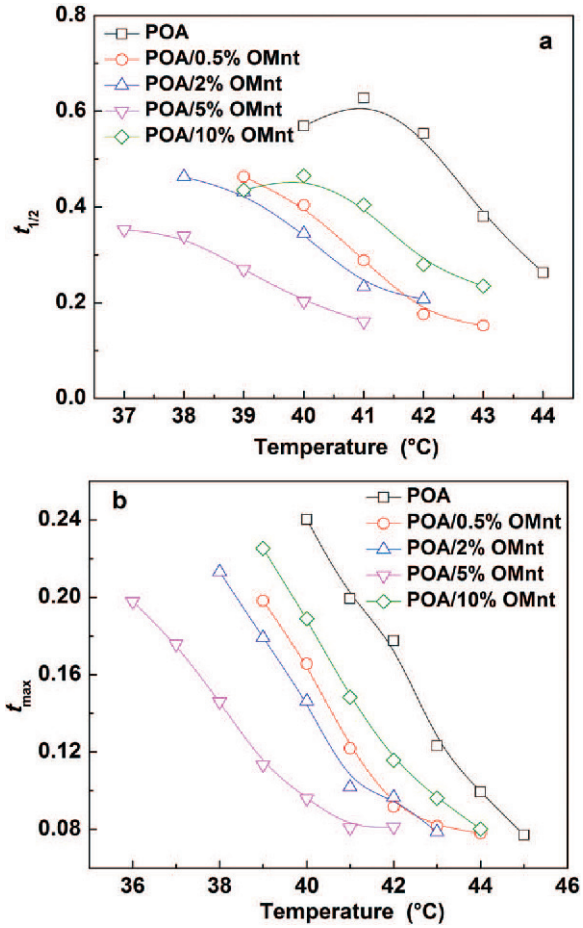

Figure 6. Crystallization half time and maximum crystallization time of the POA/OMnt composite PPD.

energy ΔE during the isothermal crystallization process can be calculated using the Arrhenius equation as shown in equation 6 (Wang *et al.*, 2003):

$$\frac{1}{n}\ln Z_t = k_0 - \frac{\Delta E}{R \cdot T_c} \quad (6)$$

where k_0 is a pre-exponential factor and R is the ideal gas constant 8.314 J·mol^{-1}·K^{-1}. Accordingly, by a linear fit of the lnZ_t *vs.* $1/T_c$ curves, the ΔE values for different composites PPDs were determined and are presented in Table 1. The ΔE value of neat POA samples was 303.328 kJ·mol^{-1}. After the addition of 0.5, 2, 5, and 10 wt.% OMnt, the ΔE values of the POA/OMnt composite PPDs decreased to 242.691, 231.999, 188.643, and 233.170 kJ·mol^{-1}, respectively, which means that adding OMnt had a dramatic impact on polymer chain motion during crystallization. Based on the crystallization kinetics, smaller ΔE values resulted in the appearance of crystalline POA polymer chains. This further confirmed that the addition of OMnt facilitated POA crystallization.

Performance of POA/OMnt composite PPDs on waxy crude oil

The pour points of the waxy crude oil with and without the addition of POA or POA/OMnt composite PPDs are illustrated in Table 3. The pour point of the waxy crude oil without POA or POA/OMnt composition PPDs was measured at 24ºC. After the addition of 50 ppm and 100 ppm POA, the pour points of the crude oil decreased to 19ºC and 14ºC, respectively. The pour points of the crude oil with 50 ppm and 100 ppm POA/5% OMnt added were further reduced to 17ºC and 11ºC, respectively. Clearly, in comparison to identical concentrations of POA, the POA/OMnt composite PPD can further inhibit the sol to gel transition of the waxy crude oil.

The transient apparent viscosity *vs.* shear rate curves at 10ºC for the treated and untreated waxy crude oils indicate (Figure 7a) that comparable amounts of the POA/OMnt composite PPD were better in decreasing the viscosity than the POA PPD. For example, at 50 s^{-1}, the

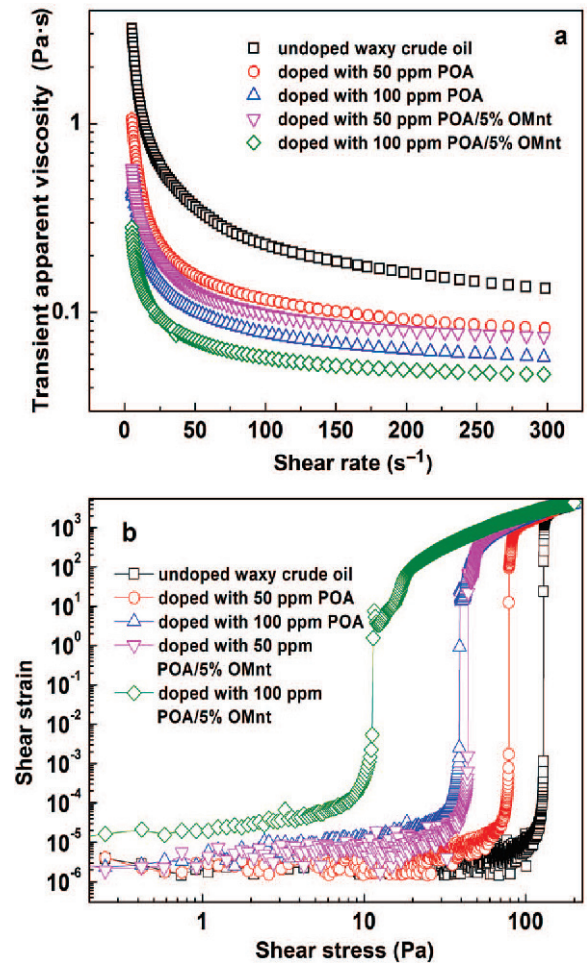

Figure 7. Transient apparent viscosity (a) and yield behavior (b) of the waxy crude oil at 10ºC with or without treatment with POA and POA/OMnt composite PPD.

https://doi.org/10.1346/CCMN.2018.064095 Published online by Cambridge University Press

apparent viscosity of the untreated waxy crude oil was 362.6 mPa·s. The addition of 50 ppm and 100 ppm POA reduced the apparent viscosity of the oil to 157.0 mPa·s and 101.3 mPa·s, respectively. The same amount of POA/OMnt composite PPD reduced the apparent viscosity to 128.6 mPa·s and 71.16 mPa·s. The average apparent viscosity reduction rates were compared in two different ways, I and II. In I, the average apparent viscosities of crude oil treated with the POA and POA/OMnt composites were compared to the untreated crude oil. In II, the average apparent viscosities of crude oil treated with POA and POA/OMnt composites were compared to the crude oil treated using the neat POA. As shown in Table 3, the average viscosity reduction rates using the addition of 50 ppm and 100 ppm POA to crude oil were 55.57% and 71.88%, respectively. The apparent viscosity values increased to 65.03% and 80.63%, respectively, using the same amounts of POA in the POA/OMnt composite PPDs as in neat POA.

The yield behaviors (Figure 7b) and the yield stresses (Table 3) of the untreated and POA and POA/Mnt composite PPD treated waxy crude oils showed that the yield stress of the untreated waxy crude oil was rather high (128.1 Pa), which means that a strong gel structure had formed. The addition of 50 ppm and 100 ppm POA weakened the gel structure of the crude oil and the yield stresses were 78.58 Pa and 38.75 Pa, respectively. Adding 50 ppm and 100 ppm of the POA/OMnt composite PPDs further weakened the gel structure of the crude oil sample and the yield stresses were 43.91 Pa and 11.25 Pa, respectively.

Polarized microscope images of the untreated and POA and POA/OMnt composite PPD treated waxy crude oil (Figure 8) were used to deduce the mechanism of POA and the POA/OMnt composite PPDs in improving the flowability of waxy crude oil. For the untreated crude oil, the precipitated wax crystals were small and very abundant, but had a haphazard arrangement (Figure 8a). After the addition of 100 ppm POA, the wax crystals started to gather into larger flocs and became more regular, which led to a substantial reduction in the number of wax crystals (Figure 8b). As a result, the solid-liquid (wax crystal-oil phase) interfacial area decreased and the trend to form a continuous 3D-wax crystal network was inhibited. Meanwhile, the structure of the wax crystal flocs appeared to be quite loose instead of compact and might occlude more liquid oil. The wax crystal structure after adding 100 ppm POA/OMnt composite PPDs became more regular and compact and the wax crystal floc sizes continuously increased (Figure 8c). This means that the POA/OMnt composite PPD could effectively act as a nucleation site to precipitate wax molecules and result in larger and more compact wax crystal flocs. The improved wax crystal morphologies (larger size and more compact), therefore, adversely affected the formation of a strong wax crystal network and improved the rheological efficiency of the POA/OMnt composite PPDs.

CONCLUSIONS

In the present work, the untreated Mnt was first modified using aqueous OTAC solution and dispersed into the POA matrix to prepare a POA/OMnt composite PPD using the melt blending method. The isothermal crystallization kinetics of the POA/OMnt composite PPDs with different OMnt contents were studied in detail using DSC. The rheological properties of the waxy crude oil were investigated by measuring the pour point, transient apparent viscosity and yield behavior, and by microscopic observation. The following conclusions were drawn: (a) The cationic surfactant OTAC molecules with eighteen side alkyl chains were successfully intercalated into the Mnt layers; (b) the OMnt and POA were compatible and the OMnt layer structures were exfoliated into several sheets in the POA matrix; (c) the chemical bonding and aggregation of POA was not affected by the OMnt; (d) the addition of OMnt facilitated POA crystallization and the crystallization half time and maximum crystallization rate first decreased as the content of OMnt (0.5~5wt.%) was increased and then increased as the content of OMnt was further increased; (e) The nucleation processes for the POA/OMnt composite PPDs with different OMnt contents were heterogeneous nucleation and the crystal growth processes were one-dimensional acicular crystal

Table 3. The performance of POA and POA/OMnt composite PPDs in reducing the pour point, average viscosity, and yield stress of waxy crude oil. Average viscosity reduction rate I and II compare the viscosities of crude oil treated with the POA and POA/OMnt composites to (I) the viscosities of untreated crude oil and (II) to the viscosities of crude oil treated with neat POA.

PPD type	Pour point (ºC)	Average viscosity reduction rate I (%)	Average viscosity reduction rate II (%)	Yield stress (Pa)
Untreated	24	–	–	128.1
50 ppm POA	19	55.57	–	78.58
50 ppm POA/5%OMnt	17	65.03	22.86	43.91
100 ppm POA	14	71.88	–	38.75
100 ppm POA/5%OMnt	11	80.63	33.33	11.25

https://doi.org/10.1346/CCMN.2018.064095 Published online by Cambridge University Press

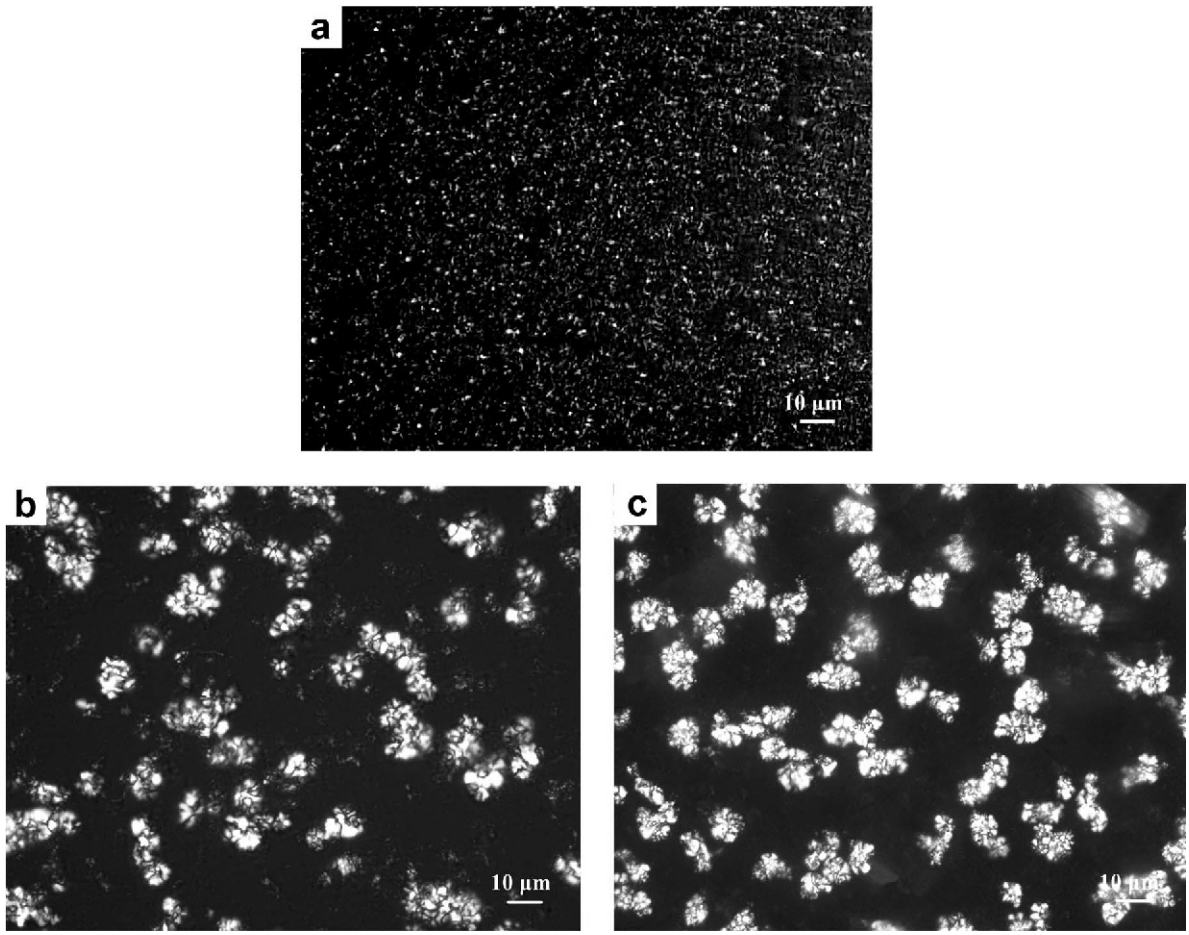

Figure 8. Polarized microscopic images at 10ºC of the waxy crude oil with and without POA and POA/OMnt composite PPD: (a) untreated; (b) with 100 ppm POA; and (c) with 100 ppm POA/5%OMnt composite PPD.

growth into two-dimensional crystals; (f) the addition of OMnt had a dramatic impact on chain motion during crystallization and finally accelerated POA crystallization; (g) after adding the POA/OMnt composite PPDs to crude oil, the mixtures exhibited better rheological properties in comparison to identical concentrations of POA; and (h) microscopic observation showed that the POA/OMnt composites acted as wax nucleation sites and resulted in larger and more compact wax crystal flocs. The wax crystals were larger and more compact and, therefore, adversely affected the formation of a strong wax crystal network, which improved the rheological properties of the POA/OMnt composite PPDs.

ACKNOWLEDGMENTS

This work was financially supported by National Natural Science Foundation of China (51774311), Natural Science Foundation of Shandong Province of China (ZR2017MEE022), Key Research Project of Shandong Province of China (GG201703230122), and by the Fundamental Research Funds for the Central Universities-China (17CX06019).

REFERENCES

Al-Sabagh, A.M., Betiha, M.A., Osman, D.I., Hashim, A.I., El-Sukkary, M.M., and Mahmoud, T. (2016) A new covalent strategy for functionalized montmorillonite–poly (methyl methacrylate) for improving the flowability of crude oil. *RSC Advances*, **6**, 109460–109472.

Avrami, M. (1940) Kinetics of phase change. II Transformation-time relations for random distribution of nuclei. *The Journal of Chemical Physics*, **8**, 212–224.

Chen, Q., Zhu, R., Ma, L., Zhou, Q., Zhu, J., and He, H. (2017) Influence of interlayer species on the thermal characteristics of montmorillonite. *Applied Clay Science*, **135**, 129–135.

He, H., Ding, Z., Zhu, J., Yuan, P., Xi, Y., Yang, D., and Frost, R.L. (2005) Thermal characterization of surfactant-modified montmorillonites. *Clays and Clay Minerals*, **53**, 287–293.

Khajehpour, M., Gelves, G.A., and Sundaraj, U. (2015) Modification of montmorillonite with alkyl silanes and fluorosurfactant for clay/fluoroelastomer (FKM) nanocomposites. *Clays and Clay Minerals*, **63**, 1–14.

Lashkarbolooki, M., Seyfaee, A., Esmaeilzadeh, F., and Mowla, D. (2010) Experimental investigation of wax deposition in Kermanshah crude oil through a monitored flow loop apparatus. *Energy & Fuels*, **24**, 1234–1241.

Li, L., Bellan, L.M., Craighead, H.G., and Frey, M.W. (2006). Formation and properties of nylon-6 and nylon-6/montmorillonite composite nanofibers. *Polymer*, **47**, 6208–6217.

https://doi.org/10.1346/CCMN.2018.064095 Published online by Cambridge University Press

Liu, C.P., Song, W.F., Lu, Q.X., and Chen, M.F. (2014) Comparison of isothermal with nonisothermal kinetics for ethylene-vinyl acetate cross-linking reaction in the solid state. *Industrial & Engineering Chemistry Research*, **53**, 10080–10089.

Oliveira, L.M., Nunes, R.C., Melo, I.C., Ribeiro, Y.L., Reis, L.G., Dias, J.C., Guimarães, R.C.L., and Lucas, E.F. (2016) Evaluation of the correlation between wax type and structure/behavior of the pour point depressant. *Fuel Processing Technology*, **149**, 268–274.

Page, K.A. and Adachi, K. (2006) Dielectric relaxation in montmorillonite/polymer nanocomposites. *Polymer*, **47**, 6406–6413.

Sadek, E.M., El-Nashar, D.E., and Ahmed, S.M. (2015) Effect of organoclay reinforcement on the curing characteristics and technological properties of styrene-butadiene rubber. *Polymer Composites*, **36**, 1293–1302.

Shi, N. and Dou, Q. (2015) Non-isothermal cold crystallization kinetics of poly (lactic acid)/poly (butylene adipate-co-terephthalate)/treated calcium carbonate composites. *Journal of Thermal Analysis and Calorimetry*, **119**, 635–642.

Shirdel Ghadikolaei, S., Omrani, A., and Ehsani, M. (2016) Impact of bacterial cellulose nanofibers on the nonisothermal crystallization kinetics of ethylene–vinyl acetate copolymer. *Industrial & Engineering Chemistry Research*, **55**, 8248–8257.

Wang, H.R., Gao, Y.L., Ye, Y.F., Min, G.H., Chen, Y., and Teng, X.Y. (2003) Crystallization kinetics of an amorphous Zr–Cu–Ni alloy: Calculation of the activation energy. *Journal of Alloys and Compounds*, **353**, 200–206.

Xu, J., Jiang, H., Li, T., Wei, X., Wang, T., Huang, J., Wang, W., Smith, A.L., Wang, J., Zhang, R., Xu, Y., Li, L., Prud'homme, R.K., and Guo, X. (2015) Effect of comb-type copolymers with various pendants on flow ability of heavy crude oil. *Industrial & Engineering Chemistry Research*, **54**, 5204–5212.

Yang, F., Paso, K., Norrman, J., Li, C., Oschmann, H., and Sjoblom, J. (2015a) Hydrophilic nanoparticles facilitate wax inhibition. *Energy & Fuels*, **29**, 1368–1374.

Yang, F., Yao, B., Li, C., Shi, X., Sun, G., and Ma, X. (2017a) Performance improvement of the ethylene-vinyl acetate copolymer (EVA) pour point depressant by small dosages of the polymethylsilsesquioxane (PMSQ) microsphere: An experimental study. *Fuel*, **207**, 204–213.

Yang, F., Yao, B., Li, C., Sun, G., and Ma, X. (2017b) Oil dispersible polymethylsilsesquioxane (PMSQ) microspheres improve the flow behavior of waxy crude oil through spacial hindrance effect. *Fuel*, **199**, 4–13.

Yang, F., Zhao, Y., Sjöblom, J., Li, C., and Paso, K.G. (2015b) Polymeric wax inhibitors and pour point depressants for waxy crude oils: A critical review. *Journal of Dispersion Science and Technology*, **36**, 213–225.

Yao, B., Li, C., Yang, F., Mu, Z., Zhang, X., and Sun, G. (2017) Effect of oil dispersible polymethylsilsesquioxane microspheres on the formation and breakage of model waxy oil gels. *Fuel*, **209**, 424–433.

Yao, B., Li, C., Yang, F., Sjöblom, J., Zhang, Y., Norrman, J., Paso, K., and Xiao, Z. (2016a) Organically modified nanoclay facilitates pour point depressing activity of polyoctadecylacrylate. *Fuel*, **166**, 96–105.

Yao, B., Li, C., Yang, F., Zhang, X., Mu, Z., Sun, G., and Zhao, Y. (2018a) Ethylene-vinyl acetate copolymer (EVA) and resin-stabilized asphaltenes synergistically improve the flow behavior of model waxy oils: 1. Effect of wax content and the synergistic mechanism. *Energy & Fuels*, **32**, 1567–1578, DOI: 10.1021/acs.energyfuels.7b03657.

Yao, B., Li, C., Yang, F., Zhang, Y., Xiao, Z., and Sun, G. (2016b) Structural properties of gelled Changqing waxy crude oil benefitted with nanocomposite pour point depressant. *Fuel*, **184**, 544–554.

Yao, B., Li, C., Zhang, X.,Yang, F., Sun, G., and Zhao, Y. (2018b) Performance improvement of the ethylene-vinyl acetate copolymer (EVA) pour point depressant by small dosage of the amino-functionalized polymethylsilsesquioxane (PAMSQ) microsphere, *Fuel*, **220**, 167–176.

Yao, B., Wang, L., Yang, F., Li, C., and Zhao, Y. (2016c). Effect of vinyl-acetate moiety molar fraction on the performance of poly (octadecyl acrylate-vinyl acetate) pour point depressants: experiments and mesoscopic dynamics simulation. *Energy & Fuels*, **31**, 448–457.

Yi, S. and Zhang, J. (2011). Shear-induced change in morphology of wax crystals and flow properties of waxy crudes modified with the pour-point depressant. *Energy & Fuels*, **25**, 5660–5671.

(*Received 11 December 2017; revised 13 April 2018; Ms. 1250; AE: Luyi Sun*)